

Comparative Study of High-Resolution RCS Models of Motorcyclists in W-Band Extracted from Measurements

Sevda Abadpour^{1,*}, Mario Pauli¹, Jan Siska², Nils Pohl², and Thomas Zwick¹

¹*Institute of Radio Frequency Engineering and Electronics (IHE)
Karlsruhe Institute of Technology (KIT), Karlsruhe 76131, Germany*

²*Institute for Integrated Systems, Ruhr-University Bochum, Bochum 44801, Germany*

ABSTRACT: Reliably modeling vulnerable road users (VRUs) such as motorcyclists in the virtual environment is indispensable in developing over-the-air (OTA) validation test methods. However, there are still challenges arising from many possible variations of VRUs, which may participate in the traffic scenarios. Therefore, it is essential to model them precisely and demonstrate consistency between virtual evaluation and reality. To achieve this goal, VRUs must be modeled based on their backscattering behavior which can be prepared based on high-resolution (HR) radar cross section (RCS) measurements. This work presents the backscattering behavior of motorcyclists as one of the critical VRUs in traffic scenarios. The extracted model of a motorcyclist is analyzed and compared based on HR-RCS measurements with different motorcycle variants. This evaluation is a prerequisite for developing a realistic model of VRUs and ensuring an adequate level of accuracy.

1. INTRODUCTION

As safety process for autonomous driving (AD) can not be ensured only by field test driving but also needs to develop a virtual environment to verify the safety assurance and reliability of advanced driver assistance system (ADAS). The automotive sensors, e.g., camera, lidar, and radar, are the components of ADAS to provide effective information and warning for AD and evaluation of its safety feature. However, each sensor type has strengths and weaknesses in the perception of the environment which can affect the functionality of the AD in object detection and recognition [2–4]. Although optical sensors can perceive the surrounding environment with high resolution, they are typically more susceptible to weather and light conditions than radar. On the other hand, with the current advancements in automotive radar technology, radar sensors can detect, track, classify, and localize the objects surrounding the host vehicle in range, azimuth, elevation, and velocity. It means that the radar sensor collects high-accuracy and high-resolution data from the environment in the 4-D domain [5]. Therefore, modern automotive radar sensors perceive the environment more realistically, consistently, and credibly [6–8]. Consequently, for evolving over-the-air (OTA) validation test methods and more consistency between the virtual validation method and reality, it is essential to prepare the HR model of radar targets [9–11] in the respective frequency range.

The HR radar models of the surrounding, especially VRUs, can be developed based on the extracted backscattering behavior from their HR-RCS measurement in the radial and angular domains. These precise radar models can be implemented in wave propagation simulations of real traffic scenarios to ap-

proach highly efficient simulation results. Accordingly, the accuracy of the simulations depends on the precision and resolution of the implemented radar models. Any failure in modeling VRUs can cause inaccuracy in the representation of reality and subsequently, safety violations of AD. There is a large variety of potential VRUs, e.g., pedestrians, cyclists, and motorcyclists, to be modeled in the simulation environment [10, 12]. Moreover, each group of them has different types. Thereby, the reliable modeling of VRUs remains challenging. It is worthwhile to analyze the backscattering model of different types of exemplary VRUs, especially those with agile behavior in traffic scenarios. This evaluation can offer a benchmark for modeling the real world and support the development and homologation of safety assurance of AD. One of the challenges for preparing the radar models based on the measured scattering points is performing the HR-RCS measurements for different viewing angles of the object under test. Consequently, repeating this measurement for all different types of VRUs is an arduous task that requires a long time.

Therefore, in this work, the HR-RCS measurement technique [11] is utilized to measure the backscattering behavior of a motorcyclist with three different types of motorcycles and extract their scattering points (SPs). Since the physical properties of the motorcycle models differ greatly, the influence on the backscattering behavior is investigated to decrease the residual risk associated with their functionality in radar simulations and machine learning algorithms.

2. MEASUREMENT SETUP

HR monostatic RCS measurement technique is employed to collect radar data from a motorcyclist with different types of

* Corresponding author: Sevda Abadpour (sevda.abadpour@kit.edu).

motorcycles and extract their radar signatures. The principle of the utilized HR-RCS measurement technique is described in [11] showing that this technique is applicable to measure different traffic objects, e.g., bicycles, pedestrians, cyclists, and motorcycles. Furthermore, the main objective in [11] is to verify the performance of the dummy object with respect to a human object so that it can replace human for long and/or dangerous test scenarios.

The HR-RCS measurement enables localizing the SPs of a motorcyclist over its body surface and the SPs' corresponding RCS values. The measurement setup is configured based on the ultra-wideband mm-wave frequency modulated continuous wave (FMCW) radar sensor [13], which is equipped with a high-focusing lens antenna and is called "Radar system" [11]. The configured working frequency range of the radar sensor is 76 GHz to 81 GHz. The mounted lens antenna to the radar sensor increases the gain of the Radar sensor to 40.5 dBi and focuses its half-power beamwidth (HPBW) of 1.3° . An exemplary measurement setup for collecting the backscattering behavior of a motorcyclist is shown in Figure 1, which is conducted in the anechoic chamber of the European Microwave Signature Laboratory (EMSL), Joint Research Center of the European Commission (JRC), Ispra, Italy.

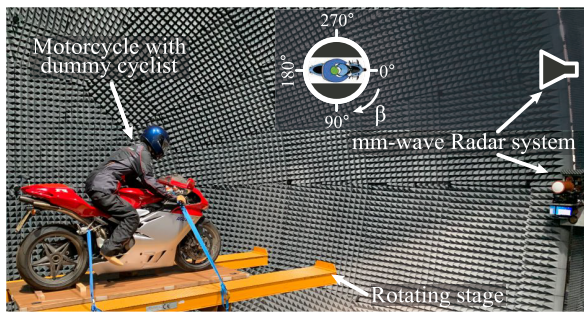


FIGURE 1. Exemplary measurement setup for monostatic RCS measurement of the motorcyclist to extract its backscattering behavior.

It should be noted that the calibration step to calculate the normalized measured RCS values is done by measuring a trihedral corner reflector (TCR) with the inner height of 10 cm. It is located in the main beam of the Radar system as a point scatterer object. Then, the RCS calibration factor is calculated by comparing the measured RCS value of the TCR and its analytical value. The analytical RCS value [14] of the utilized TCR is 14.57 dBsm, and its measured value is 15.33 dBsm. Therefore, the RCS calibration value for the presented measurement in this work is -0.75 dB.

To extract the motorcyclists' radar model, a human dressed in a motorcycle combi suit must sit still on a motorcycle for a relatively long time to scan it in its different azimuthal rotation angles (β). The investigation for the radar model of a person and a dummy human of the same size shows that they have similar backscattering behavior [11]. Accordingly, a person rider is replaced by a dummy rider, which is dressed in a motorcycle combi suit, during the measurements. The motorcyclist is placed on the rotating stage, which moves counterclockwise to scan the motorcyclist with the favorite azimuthal resolution an-

gle ($\Delta\beta = 10^\circ$). The center of the motorcyclist is placed in the range of $R = 9$ m from the antenna feed of the Radar system. The mechanical specification of the measurement setup authorizes the Radar system to scan the whole dimension of the motorcyclist in elevation and azimuth direction with a step width of 1° . Subsequently, a complete 360° HR-RCS measurement is performed on the motorcyclist to detect its scattering points from different viewing angles (β). More details of the measurement setup and the signal processing chain for determining the SP matrix are discussed in [11].

3. MEASUREMENT RESULTS

A validated dummy motorcyclist is mounted in the test setup, which is explained in Section 2, to extract its scattering points from various viewing angles of the radar. The dummy motorcyclist is a rider of three different types of motorcycles, i.e., classic (Honda 900 Hornet), sport (MV Augusta), and cross (Honda XL 250S), during the experiments. The Radar system initially begins to measure the backscattered signals by illuminating the dummy motorcyclist from the front side. The front side of the motorcyclist under test corresponds to the radar viewing angle of $\beta = 0^\circ$. Figure 2 shows the extracted radar models of the measured motorcyclists, i.e., same rider for each type of the motorcycle under experiment, from their viewing angles in the front view ($\beta = 0^\circ$), side view ($\beta = 90^\circ$), and back view ($\beta = 180^\circ$), respectively. The measurement results for full azimuthal rotation angles of motorcyclists are examined for the approximation of their outline, orientation, and dimensions. The outline and orientation of the cyclist with each motorcycle are recognizable correctly from the extracted radar images. Furthermore, the type of motorcycle is distinguishable in the extracted images.

For quantitative analysis, the derived dimensions of the reconstructed models are compared with the motorcyclist's corresponding actual sizes ($L \times W \times H$). The actual geometrical sizes of the motorcyclist are $2.2 \text{ m} \times 0.8 \text{ m} \times 1.96 \text{ m}$ with classic, $1.9 \text{ m} \times 0.8 \text{ m} \times 1.7 \text{ m}$ with sport, and $2.17 \text{ m} \times 0.87 \text{ m} \times 1.85 \text{ m}$ with cross motorcycle. Correspondingly, their measured dimensions from extracted radar images are $2.5 \text{ m} \times 0.95 \text{ m} \times 1.89 \text{ m}$, $1.93 \text{ m} \times 0.78 \text{ m} \times 1.42 \text{ m}$, and $2.11 \text{ m} \times 0.94 \text{ m} \times 1.58 \text{ m}$. It is concluded that the measured and actual sizes are in good agreement according to the accuracy and resolution [11] of the measurement setup.

For investigation of the influence of the motorcycle type on the backscattering behavior of the motorcyclist, the RCS values of the extracted SPs are averaged in each azimuthal rotation angle, and these values are shown in Figure 3. As expected, this figure clearly illustrates that the motorcyclist with a classic and cross motorcycle has a stronger scattering in comparison with riding a sport type. This observation is the effect of the bigger physical size and more metallic material in the structure of the classic and cross motorcycles on their reflectivity behavior. The differences between averaged RCS values of the motorcyclist with different types in similar viewing angles are inspected, and the maximum observed value is 4 dB. Besides, the sensitivity of the measurements is inspected through Figure 4. It shows the scattered plot of RCS values for the cross motorcy-

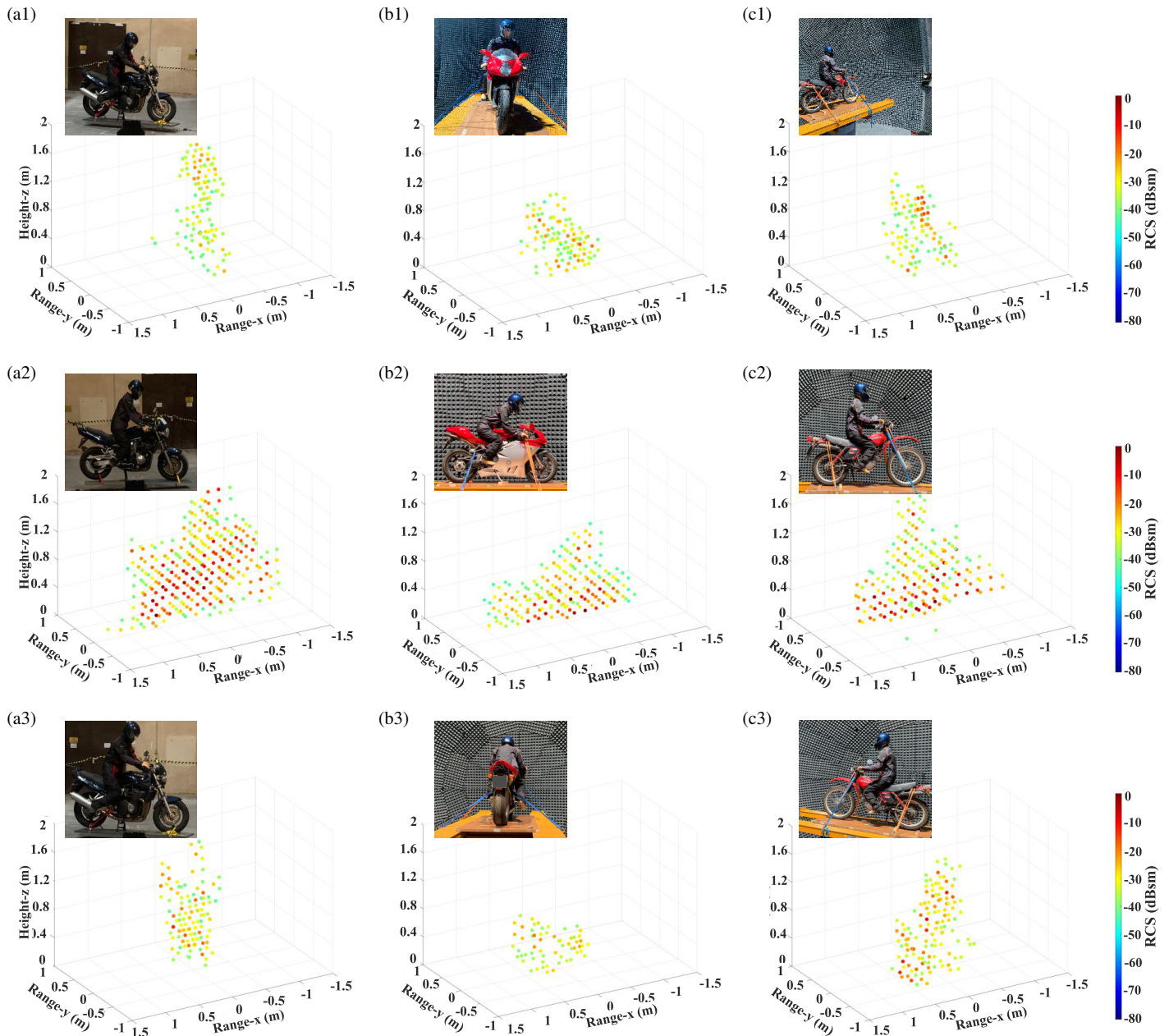


FIGURE 2. Extracted radar model of a motorcyclist with different type of motorcycles in front view ($\beta = 0^\circ$) of (a1) classic, (b1) sport, (c1) cross motorcycle; left side view ($\beta = 90^\circ$) of (a2) classic, (b2) sport, (c2) cross motorcycle; and rear view ($\beta = 180^\circ$) of (a3) classic, (b3) sport, (c3) cross motorcycle.

cle together with the corresponding average in azimuthal angle as a solid line. The sensitivity of the measurements can be observed through points with high RCS values.

For a more detailed analysis, a dedicated algorithm is developed to calculate the RCS pattern of the measured motorcyclist when it is considered as a single scattering point from the extracted radar model. The signal processing chain of the algorithm is shown in Figure 5. The inputs of the algorithm are the sampled IF data $[S_{if}(\phi_{ij}, \theta_{ij}, \beta_j)]$, which is collected from measuring the object under test in every azimuthal rotation angle (β_j) with a step width of $\Delta\beta$ to cover the whole 360° viewing angle. The Radar system scans each viewing side of

the object under test in the range of $\pm\varphi_{ij}$ in azimuth and $\pm\theta_{ij}$ in elevation directions with a step width of 1° . It ensures that the whole dimension of the object under test is scanned. Then, the algorithm explained in [11] is applied for extracting the scattering point matrix in every azimuthal rotation angle to calculate the related scattering point matrix ($\mathbf{SP}(\beta_j)$) in which its rows have the following structure:

$$\vec{SP}(\beta_j) = [x''_{ij} \quad y''_{ij} \quad z''_{ij} \quad \text{RCS}_{ij} \quad \varphi_{ij} \quad \theta_{ij} \quad \overline{sl}_{ij}] \quad (1)$$

where x''_{ij} , y''_{ij} , z''_{ij} are the coordinates of the i th scattering point on the object under test extremities in viewing angles β_j ; RCS_{ij} is its measured RCS value; and \overline{sl}_{ij} is its measured

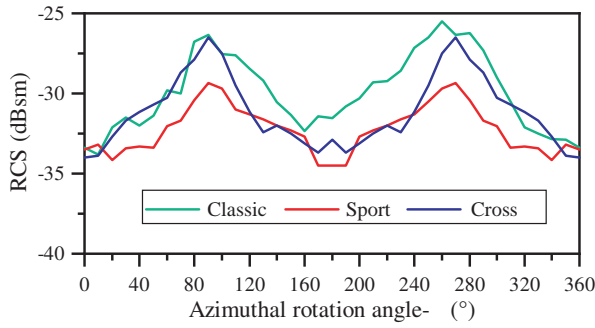


FIGURE 3. The corresponding average RCS values of the motorcyclist with a different types of motorcycles in different azimuthal rotation angles (β).

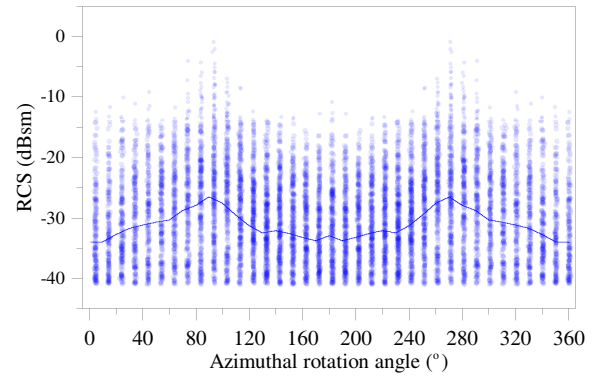


FIGURE 4. The measured RCS values of different scattering points for the motorcyclist with a cross motorcycle in each azimuthal angle (β). Dots show the measured RCS values and the solid line shows the calculated average of the measured RCS value in the corresponding angle.

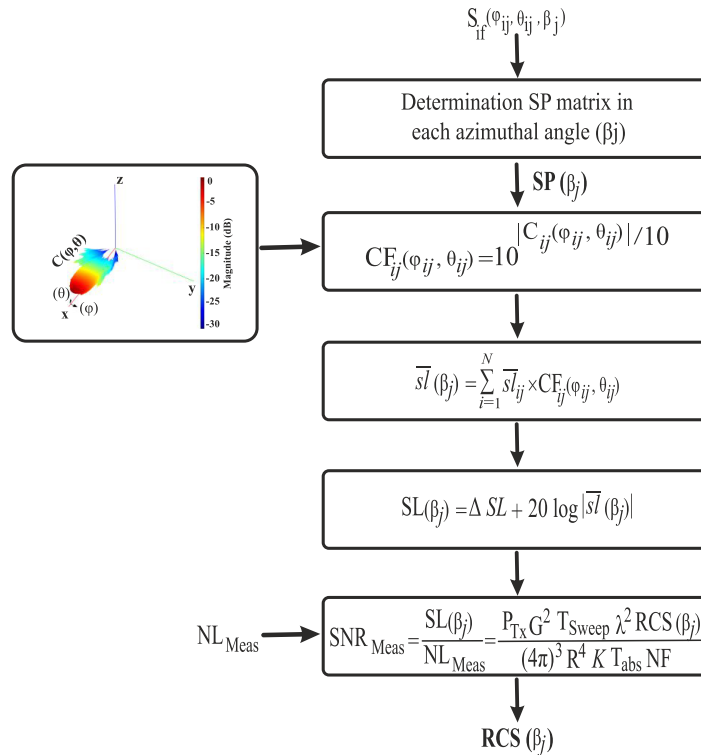


FIGURE 5. Signal processing chain for calculating the RCS pattern of the measured object from its extracted SPs in different azimuthal rotation angles (β).

signal level. It should be noted that the RCS value of the i th scattering point is calculated based on the previously measured noise level (NL_{Meas}) of the Radar system. Subsequently, the algorithm produces the correction factor of the received signal level (CF_{ij}) based on the scanning area (φ_{ij} and θ_{ij}) and measured normalized two-way radiation pattern of the radar sensor [$C_{ij}(\varphi_{ij}, \theta_{ij})$] in the absence of the high focusing lens. In the next step, the algorithm sums up the complex signal level of the object under test, which is corrected by the calculated correction factor. To approximate the magnitude of the signal in each β_j when the object under test is assumed to be a

point scatterer ($SL(\beta_j)$), a calibration factor (ΔSL) of the estimated signal is necessary. For this purpose, an experiment for detecting a point scattering object (TCR with the inner height of 4.4 cm) in the presence of the high focusing lens antenna is conducted. The TCR is placed at a distance of 9.12 m from the sensor. The main beam of the Radar system is aligned with the center of the TCR, and the raw data is collected for these measurements. Then, the dielectric lens antenna is removed from the test setup, and the measurements are repeated to collect the raw data as well. The collected raw data is depicted in Figure 6 to compare the detected signal level in the absence

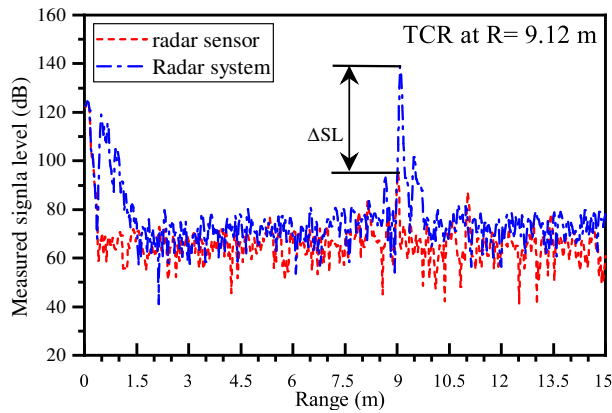


FIGURE 6. Measured reflected signal from a TCR with the size of 4.4 cm which is positioned at the range of 9.12 m from the radar sensor in the two experiments, i.e., measuring with lens antenna and measuring after removing the lens antenna. A comparison between the Radar sensor and radar system shows the gain [1].

($SL_{ab,L}$) and presence ($SL_{pr,L}$) of the lens. Since the Radar system, the radar equipped with the lens antenna, has a gain of 40.5 dBi, the expected difference between the detected signal levels (ΔSL) in the mentioned experiments is around 40.5 dBi. The calculated ΔSL from the measured signal levels in Figure 6 is 41 dB which is in good agreement with the expected value. Furthermore, the gain of the Radar system can be predicted by comparing the magnitude of the two mentioned measurements and with the following equation,

$$G_{\text{Radar system}} = G_{\text{radar}} + \frac{1}{2} \Delta SL = 20 \text{ dBi} + \frac{1}{2} \Delta SL \quad (2)$$

and

$$\Delta SL = SL_{ab,L} - SL_{pr,L} \quad (3)$$

where $SL_{ab,L}$ and $SL_{pr,L}$ are the detected signal levels in the absence and presence of the lens, respectively. Subsequently, ΔSL is calculated by comparing the received signal level of measuring a TCR in the absence and presence of a focusing lens antenna which is estimated as 41 dB.

Consequently, the estimated RCS value in each azimuthal rotation angle ($(\text{RCS}(\beta_j))$) can be calculated by radar equation [11] and its estimated signal to noise ratio level (SNR_{Meas}). The estimated RCS pattern from the collected raw data in HR-RCS measurement is depicted in Figure 7 for the motorcyclist with different types of motorcycles. As expected, the RCS values of the motorcyclist in the side views ($\beta = 90^\circ$ & 270°) are more robust than the front or back side. The estimated RCS values over the motorcyclist azimuthal angle change between -20 and 7 dBsm, which are expected values based on the reported values in [15, 16]. It is worth mentioning that Figure 3 shows the averaged measured RCS values of extracted SPs while the object under test is assumed as a set of multiple scattering points. However, in Figure 7, the object under test is considered as a single scattering point. Therefore, the reported RCS values for various azimuthal angles in each plot are different.

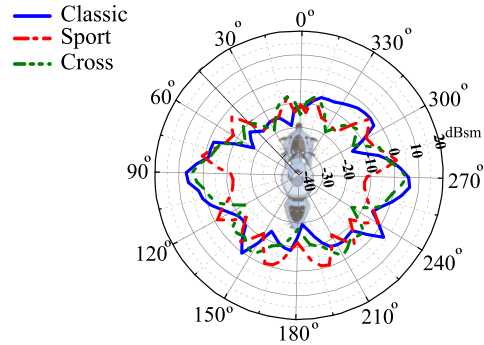


FIGURE 7. Calculated RCS pattern for the measured dummy motorcyclist utilizing different types of motorcycles from its different viewing angles (β) based on the explained algorithm [1].

4. CONCLUSION

This letter presents a comparative analysis of the backscattering behavior of a motorcyclist riding different types, i.e., classic, sport, and cross, of motorcycles. According to the results, a motorcyclist with different types of motorcycles has roughly similar backscattering behavior, and the RCS values of the SPs in the extracted radar models are analogous. The approximated RCS patterns of the motorcyclist, from its HR extracted radar models, show that the motorcycle type does not significantly influence its overall reflectivity behavior. It can only change the level of the RCS values in different viewing angles. To the best of the authors' knowledge, for the first time measurements of different motorcycles have been compared and analyzed. It is shown that despite the differences in the motorcycle type, a general model might be derived from the measurement of one single type, and -if desired- by reducing the broad side RCS in the case of a sporty model. These general models can be used for implementation in radar simulations or as a basis for generic models. Therefore, it can be concluded that measuring every type of motorcycle is not necessary for developing realistic radar models of motorcyclists for later implementation in wave propagation simulations. It is adequate to measure the motorcyclist with one of the types and prepare a general realistic model of motorcyclists.

ACKNOWLEDGEMENT

This work was supported by the German Federal Ministry of Education and Research (BMBF) through the VIVID Project under Grant 16ME0171. Moreover, the authors thank J. Fortuny from the European Microwave Signature Laboratory, the Joint Research Center of the European Commission, Ispra, Italy, for providing the test environment.

REFERENCES

- [1] Abadpour, S., *Modeling Backscattering Behavior of Vulnerable Road Users Based on High-resolution Radar Measurements*,

- Vol. 103, 158, KIT Scientific Publishing, Nov. 2023.
- [2] Vargas, J., S. Alsweiss, O. Toker, R. Razdan, and J. Santos, "An overview of autonomous vehicles sensors and their vulnerability to weather conditions," *Sensors*, Vol. 21, No. 16, 5397, Aug. 2021.
- [3] Zang, S., M. Ding, D. Smith, P. Tyler, T. Rakotoarivelo, and M. A. Kaafar, "The impact of adverse weather conditions on autonomous vehicles: How rain, snow, fog, and hail affect the performance of a self-driving car," *IEEE Vehicular Technology Magazine*, Vol. 14, No. 2, 103–111, Jun. 2019.
- [4] Heinzler, R., P. Schindler, J. Seekircher, W. Ritter, and W. Stork, "Weather influence and classification with automotive lidar sensors," in *2019 IEEE Intelligent Vehicles Symposium (IV)*, 1527–1534, Paris, France, Jun. 2019.
- [5] Murad, M., I. Bilik, M. Friesen, J. Nickolaou, J. Salinger, K. Geary, and J. S. Colburn, "Requirements for next generation automotive radars," in *2013 IEEE Radar Conference (RadarCon13)*, 1–6, Ottawa, Canada, 2013.
- [6] Dubey, A., A. Santra, J. Fuchs, M. Luebke, R. Weigel, and F. Lurz, "A Bayesian framework for integrated deep metric learning and tracking of vulnerable road users using automotive radars," *IEEE Access*, Vol. 9, 68 758–68 777, 2021.
- [7] Dickmann, J., N. Appenrodt, H.-L. Bloecher, C. Brenk, T. Hackbarth, M. Hahn, J. Klappstein, M. Muntzinger, and A. Sailer, "Radar contribution to highly automated driving," in *2014 44th European Microwave Conference*, 1715–1718, Rome, Italy, Oct. 2014.
- [8] Waldschmidt, C. and H. Meinel, "Future trends and directions in radar concerning the application for autonomous driving," in *2014 11th European Radar Conference*, 1719–1722, Rome, Italy, Oct. 2014.
- [9] Abadpour, S., M. Pauli, C. Schyr, F. Klein, R. Degen, J. Siska, N. Pohl, and T. Zwick, "Angular resolved RCS and Doppler analysis of human body parts in motion," *IEEE Transactions on Microwave Theory and Techniques*, Vol. 71, No. 4, 1761–1771, Apr. 2023.
- [10] Schubert, E., F. Meinel, M. Kunert, and W. Menzel, "High resolution automotive radar measurements of vulnerable road users — Pedestrians & cyclists," in *2015 IEEE MTT-S International Conference on Microwaves for Intelligent Mobility (ICMIM)*, 1–4, Heidelberg, Germany, Apr. 2015.
- [11] Abadpour, S., S. Marahrens, M. Pauli, J. Siska, N. Pohl, and T. Zwick, "Backscattering behavior of vulnerable road users based on high-resolution RCS measurements," *IEEE Transactions on Microwave Theory and Techniques*, Vol. 70, No. 3, 1582–1593, Mar. 2022.
- [12] Reyes-Muñoz, A. and J. Guerrero-Ibáñez, "Vulnerable road users and connected autonomous vehicles interaction: A survey," *Sensors*, Vol. 22, No. 12, 4614, Jun. 2022.
- [13] Pohl, N., T. Jaeschke, S. Küppers, C. Bredendiek, and D. Nüßler, "A compact ultra-wideband mmWave radar sensor at 80 GHz based on a SiGe transceiver chip (Focused session on highly-integrated millimeter-wave radar sensors in SiGe BiCMOS technologies)," in *2018 22nd International Microwave and Radar Conference (MIKON)*, 345–347, Poznan, Poland, May 2018.
- [14] Richards, M. A., J. A. Scheer, and W. A. Holm, *Principles of Modern Radar: Basic Principles*, SciTech Publishing, Inc., 2010.
- [15] Geary, K., J. S. Colburn, A. Bekaryan, S. Zeng, B. Litkouhi, and M. Murad, "Automotive radar target characterization from 22 to 29 GHz and 76 to 81 GHz," in *2013 IEEE Radar Conference (RadarCon13)*, 1–6, Ottawa, ON, Canada, Apr. 2013.
- [16] Köhler, M., J. Hasch, H. L. Blöcher, and L.-P. Schmidt, "Feasibility of automotive radar at frequencies beyond 100 GHz," *International Journal of Microwave and Wireless Technologies*, Vol. 5, No. 1, 49–54, Feb. 2013.